RESEARCH ARTICLE | SEPTEMBER 01 1990

Chaos in Maps with Continuous and Discontinuous Maxima: A dramatic variety of dynamic behavior is revealed by graphical display of the Lyapunov exponent

Mario Markus

Comput. Phys. 4, 481–493 (1990)
https://doi.org/10.1063/1.4822940

Chaos in Maps with Continuous and Discontinuous Maxima

Mario Markus

A dramatic variety of dynamic behavior is revealed by graphical display of the Lyapunov exponent

A graphical technique for the display of the Lyapunov exponent as a function of control parameters in one-dimensional maps is used to identify coexistence of attractors, superstable curves, highly interleaved basins of attraction in phase space, and highly interleaved regions with different oscillatory modes in parameter space. Furthermore, this technique reveals dramatic changes of dynamic behavior due to small discontinuities at the maximum of the maps.

Introduction

A number of natural phenomena can be described by maps of the type $x_{n+1} = f(x_n)$, the most extensively studied example being the logistic equation

$$x_{n+1} = r\ x_n\ (1 - x_n) \tag{1}$$

(For reviews of the dynamic properties of this map, see References 1, 2.) The choice of this example is not very restrictive, since any application $g:[a,b] \rightarrow [a,b]$ with $g(a) = g(b) = a$ and with one parabolic maximum in [a,b] is topologically conjugated to the logistic map, thus exhibiting analogous dynamic features (see References 3, 4). References dealing with physical, chemical and biological examples of maps such as g are given in References 5–8.

A dramatically different dynamic behavior is obtained if a map with the properties of g is perturbed by a discontinuity at its maximum. One example of a map with such a discontinuity, which has been studied in References 9, 10, is

$$y_{n+1} = 1 - R\ y_n^2 \quad \text{if } y_n > 0 \tag{2a}$$

$$y_{n+1} = \alpha - R\ y_n^2 \quad \text{if } y_n \leqslant 0. \tag{2b}$$

This type of map occurs in appropriate Poincaré sections of the Lorenz model, well known to reflect dominant convective properties of fluids[11].

Introducing a transformation of variables in Eqs. (2) such that the interval [0,1] is mapped into itself (as in Eq. (1)) leads to

$$x_{n+1} = r\ x_n\ (1 - x_n) \quad \text{if } x_n > 0.5 \tag{3a}$$

$$x_{n+1} = r\ x_n\ (1 - x_n) + \tfrac{1}{4}(\alpha - 1)(r - 2) \quad \text{if } x_n \leqslant 0.5. \tag{3b}$$

Mario Markus leads a research group at the Max Planck Institute (Rheinlanddamm 201, D-4600 Dortmund 1, Germany) and teaches Physics at the University of Dortmund.

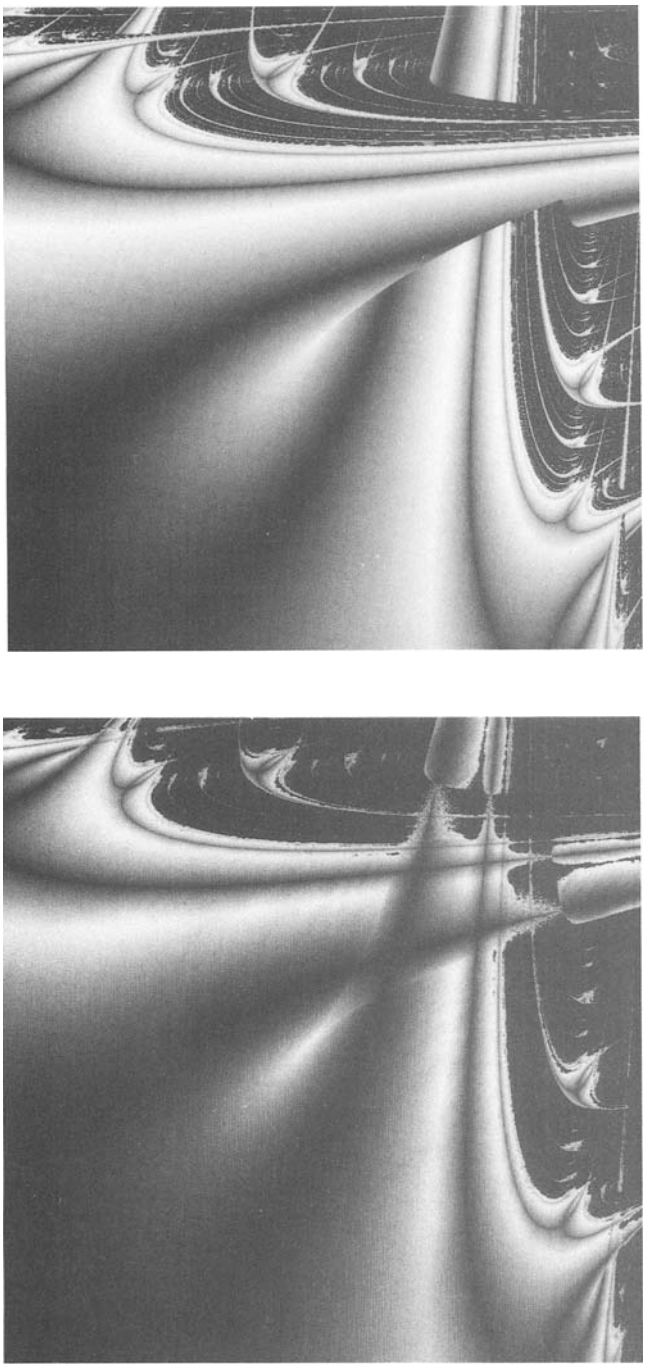

Fig.1: λ from Eq. (4). Abscissa, B; ordinate, A. Ranges: $2 \leqslant A,B \leqslant 4$. $p_A = p_B = 0.5$ (a) (upper) $p_{A|B} = 1$, i.e. $\{r_n\} = \{BABA...\}$; (b) (lower) $p_{A|B} = 0.99$. Both (a) and (b) are from References 6, 7.

In this paper the effect of a modulation of maps (1) and (3), assuming a time-dependent parameter r, will be studied. In natural systems, this means that the environmental conditions (for example the light intensity in a photosensitive system) change in time. Thus, r_n instead of r is set in Eqs. (1) and (3), yielding

$$x_{n+1} = r_n \; x_n \; (1 - x_n) \tag{4}$$

for the continuous map, and

$$x_{n+1} = r_n \; x_n \; (1 - x_n) \text{ if } x_n > 0.5 \tag{5a}$$

$$x_{n+1} = r_n \; x_n \; (1 - x_n) + \tfrac{1}{4} (\alpha - 1) \; (r_n - 2) \text{ if } x_n \leqslant 0.5 \tag{5b}$$

for the discontinuous map.

In order to include a minimum number of variables in the analysis, a dichotomic hypothesis is made, allowing r_n to assume only two values A and B. The sequence of A's and B's may be periodic or random. In previous investigations [5-8] only Eq. (4) was studied on the A-B-plane. Here, Eq. (4) is revisited, including sequences $\{r_n\}$ not considered before. Furthermore, the present work deals for the first time with the effects of discontinuities at the maximum of the map, scanning the A-B-plane with Eqs. (5) at different values of α and different sequences $\{r_n\}$.

Method of Analysis and Graphical Display

For quantification of chaos and order, the Lyapunov exponent

$$\lambda = \lim_{N \to \infty} \frac{1}{N} \sum_{n=1}^{N} \log_2 \left| \frac{d \, x_{n+1}}{d \, x_n} \right| \tag{6}$$

is calculated. Unless stated otherwise, the "seed", i.e. the first value of the iteration, is set to $x_0 = 0.5$ in this work. Order (i.e. predictability) is indicated by $\lambda < 0$. Chaos (i.e. sensitive dependence on initial conditions) is indicated by $\lambda > 0$.

Double precision arithmetic was used throughout the work. The random sequences of r_n were produced by a random number generator (routine FA01AS from the Harwell Subroutine Library[12]). Before applying Eq. (6), starting the count with $n = 1$, 600 iterations were performed in order to allow transients to die away. The first value of these 600 iterations was set equal to x_0. Satisfactory convergence of λ was achieved by setting $N = 4 \times 10^3$.

In the half-tone and color pictures, λ is represented on the A-B-plane. The grey level or color at each (A,B)-pair indicates the value of λ at that pair. The significance of the colors is indicated in the figure captions. In the half-tone pictures, the grey level changes from black to white as λ increases from $-\infty$ to 0. In order to clearly visualize the transition from order ($\lambda < 0$) to chaos ($\lambda > 0$) in Figs.1 to 7 and in Fig.14, the grey level jumps from white to black at $\lambda = 0$ and stays black for $\lambda > 0$. In contrast, Figs.10 to 13 and Figs.17 to 24 do not show such a discontinuity: the grey level changes smoothly from white to black as λ increases from zero to its maximum value. This latter distribution of shadings permits us to visualize structures not only in the ordered regions, but also in the chaotic regions.

As a help for a better understanding of the half-tone pictures, it is worth mentioning that in general the "motifs" in the picture foregrounds correspond to order ($\lambda < 0$), and the picture backgrounds to chaos ($\lambda > 0$). Superstable curves ($\lambda \to -\infty$) appear as dark lines within the "motifs" in the foregrounds. (For a discussion on superstable curves for other maps, see References 4, 13.)

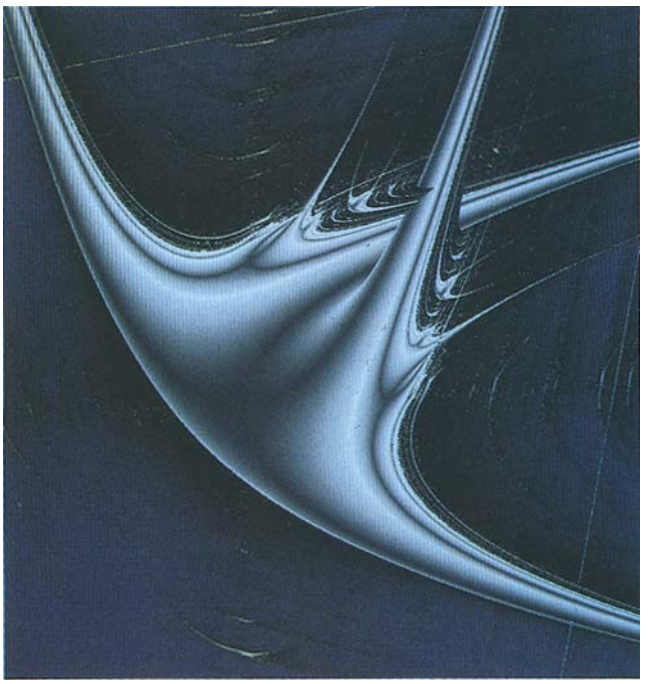

Fig.2: λ from Eq. (4). $\{r_n\}=\{BABA...\}$ Abscissa, B; ordinate, A. Ranges: $3.808 \leqslant A,B \leqslant 3.867$; (from Reference 5). The color changes from blue to white as λ increases from $-\infty$ to zero, and from black to blue as λ increases from zero to its maximum value.

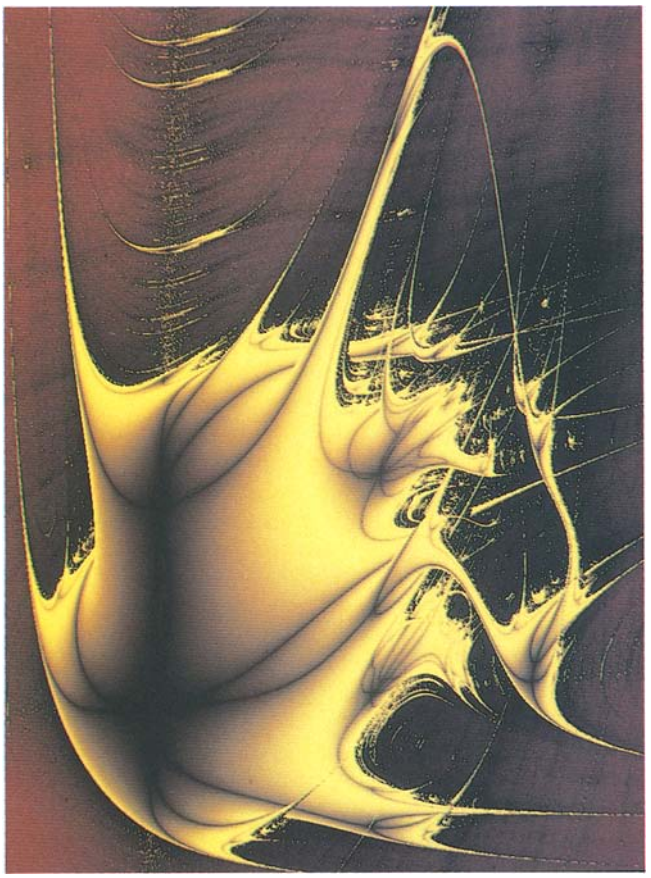

Fig.3: λ from Eq. (4). $\{r_n\}=\{BBABA\ BBABA...\}$. Abscissa, B; ordinate, A. Ranges: $3.8225 \leqslant A \leqslant 3.8711$, $3.8218 \leqslant B \leqslant 3.8607$. The color changes from black to yellow as λ increases from $-\infty$ to zero, and from black to red as λ increases from zero to its maximum value.

Results for a Modulated Continuous Map (Logistic Equation)

Coexistence of attractors and self-similarity

A number of results for the modulated logistic equation (4) have been presented in previous works [5-8]. With a few exceptions, I will focus on aspects not discussed before.

Fig.1a shows the Lyapunov exponent λ on the A-B-plane for the sequence $\{r_n\}=\{BABABA...\}$[6, 7]. The graphical display technique used here allows the straightforward identification of coexisting attractors, such as in the upper right of this figure. Here, two branches overlap: one going from left to right, "lying above" another one going upwards. In the overlapping region, two attractors coexist. Fig.1b shows the results for the same conditions as Fig.1a, except that a small degree of randomness is introduced by setting the conditional probability $p_{A|B}=0.99$. The random changes between the sequences ...BABABA... and ...ABABAB... in Fig.1b destroy the asymmetry which appears in Fig.1a with respect to the main diagonal A = B. Some special aspects of Fig.1b will be discussed later in this article.

Fig.4: λ from Eq. (4). $\{r_n\}=\{BBABABA\ BBABABA...\}$. Abscissa, B; ordinate, A. Ranges: $3.8215 \leqslant A,B \leqslant 3.8553$.

Fig. 2 shows an enlargement of the period-3 window within the chaotic region of the upper part of Fig.1a. Fig.2, together with Fig.1a, clearly demonstrates the self-similar properties of these diagrams. Self-similarity on a two-dimensional parameter space has also been found for circle maps[14,15]. The effect of a change in the pattern sequence on the period-3 window is shown in Fig.3 ($\{r_n\}=\{BBABA\ BBABA...\}$) and Fig.4 ($\{r_n\}=\{BBABABA\ BBABABA...\}$). Note the increasing number of crossings of superstable lines ongoing from Fig.2 to Fig.3 and then to Fig.4. More complex structures are found in Fig.5 ($\{r_n\}=\{B^6A^6\ B^6A^6...\}$). Fig.6 (same sequence as Fig.4, but different region of the A-B-plane) shows two overlapping swallow-shaped structures (such

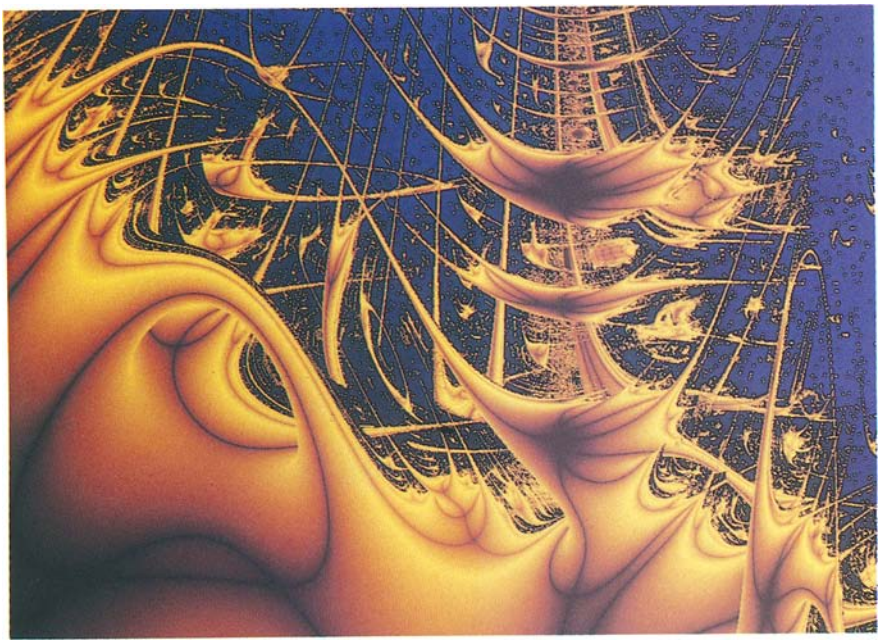

Fig.5: λ from Eq. (4). $\{r_n\}=\{B^6A^6\ B^6A^6...\}$. Abscissa, B; ordinate, A. Ranges: $3.3936 \leqslant A \leqslant 4$, $2.516 \leqslant B \leqslant 3.647$; (from Ref. 5). The color changes from black to yellow as λ increases from $-\infty$ to zero, and from black to blue as λ increases from zero to its maximum value.

as that in Fig.2) in the upper right. These overlapping structures can be inspected in detail in an enlarged portion of Fig.6, which is given in Fig.7a. One can see in Fig.7a that three attractors coexist, as indicated by the overlapping of three branches slightly above and slightly to the left of the picture center. Fig.7b shows an enlargement of this region of threefold coexistence.

Highly interleaved regions in parameter space and in phase space

In the upper right region of Fig.7b an exceptional situation is detected: two branches overlap, but none of them is clearly above the other, as for example in Fig.1a. Instead, the branches mix in a "fuzzy" way. To make sure

Fig.6: λ from Eq. (4). $\{r_n\}=\{BBABABA\ BBABABA...\}$. Abscissa, B; ordinate, A. Ranges: $3.212 \leqslant A \leqslant 4$, $2.759 \leqslant B \leqslant 3.744$ (from Ref. 6). The color changes from black to yellow as λ increases from $-\infty$ to zero, and from black to blue as λ increases from zero to its maximum value.

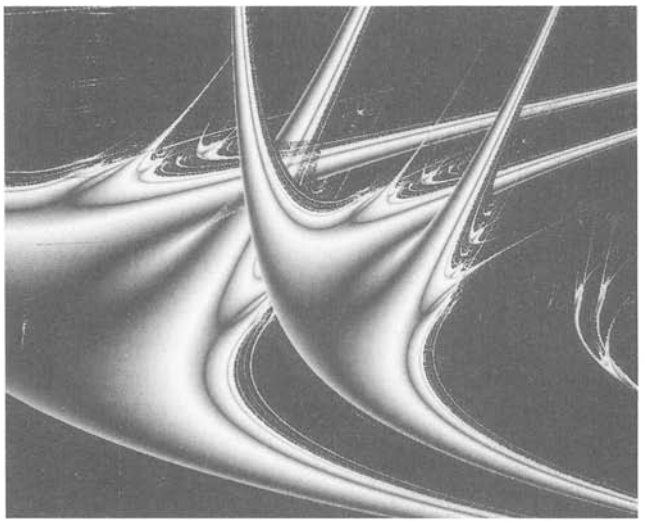

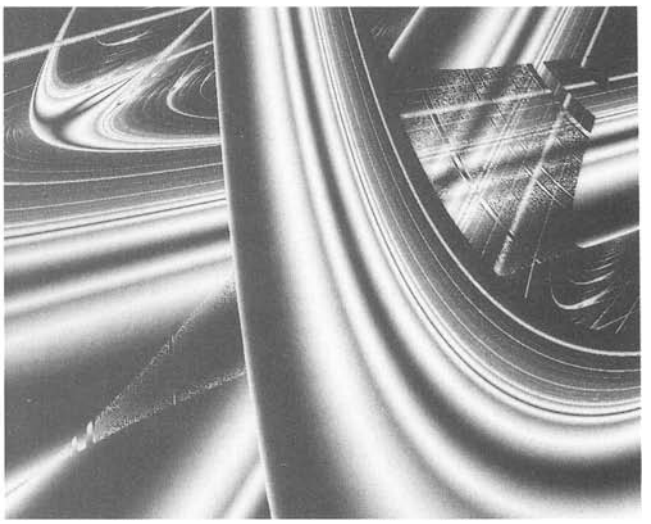

Fig.7: λ from Eq. (4). $\{r_n\}=\{$BBABABA BBABABA...$\}$. Abscissa, B; ordinate, A. (a) (left) Ranges: $3.7906 \leqslant A \leqslant 3.865279$, $3.5576 \leqslant B \leqslant 3.650967$; (b) (right) Ranges: $3.8308 \leqslant A \leqslant 3.8471$, $3.5842 \leqslant B \leqslant 3.605$.

that this fuzziness was not due to numerical errors, a recalculation was done with a higher accuracy, and the picture did not change. A clarification of the fuzziness is given in Figs.8 and 9. In fact, Fig.8a shows the Lyapunov exponents λ_1 and λ_2 for the coexisting (periodic) attractors as a function of the seed x_0. The enlarged portion in Fig.8b illustrates the high interleaving of the basins of these attractors in phase space, and the self-similar character of these basins. Fig.9, which is to be compared with Fig.8b, illustrates the sensitive dependence

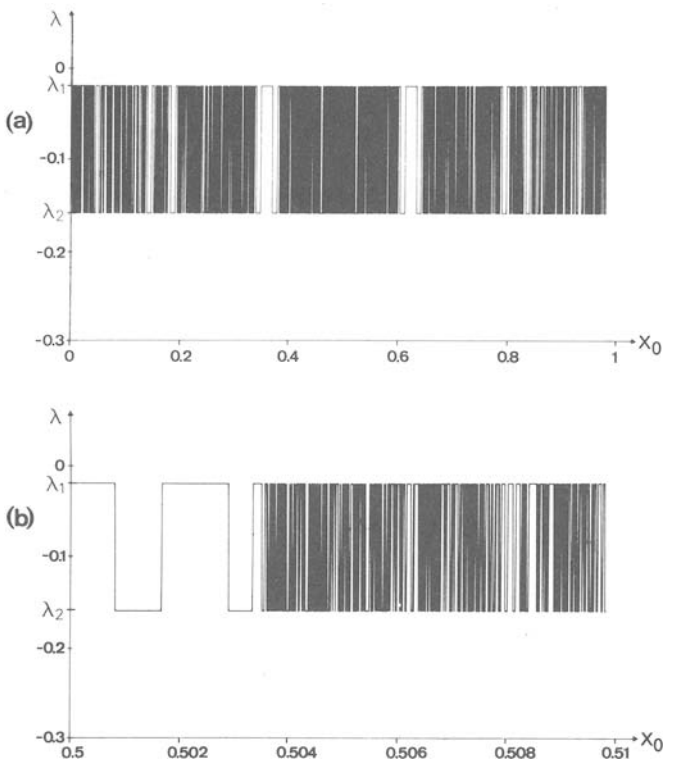

Fig.8: λ as a function of the seed x_0. A=3.5988, B=3.8420. Two periodic attractors coexist, corresponding to λ_1 and λ_2. (b) is an enlarged portion of (a).

of these basins on the control parameters. In fact, changes of a control parameter (A in this case) of about one per million causes shifts of these basins in such a way that different attractors are obtained for the same seed. For example, if $x_0 = 0.5$, one obtains λ_1 for $A = 3.5988$ (Fig.8b), λ_2 for $A = 3.598805$ (Fig.9a) and λ_1 for $A = 3.598810$ (Fig.9b). Such changes between λ_1 and λ_2 upon small changes in the control parameters cause fuzziness in the function λ (A,B), as illustrated in Fig.7b.

While Fig.7 shows that different periodic regions may be highly interleaved in parameter space (A-B-plane), Figs.10 to 13 show high interleaving of regions of order and chaos in this space. This phenomenon is especially dramatic in Figs. 12 and 13. These pictures reveal a nesting of periodic rings within each other. Chaos occurs between the rings and a superstable curve lies within each ring. Here, very small changes of A or B (of the order of 10^{-5}) cause jumps between extremely different dynamic behaviors: superstability and chaos.

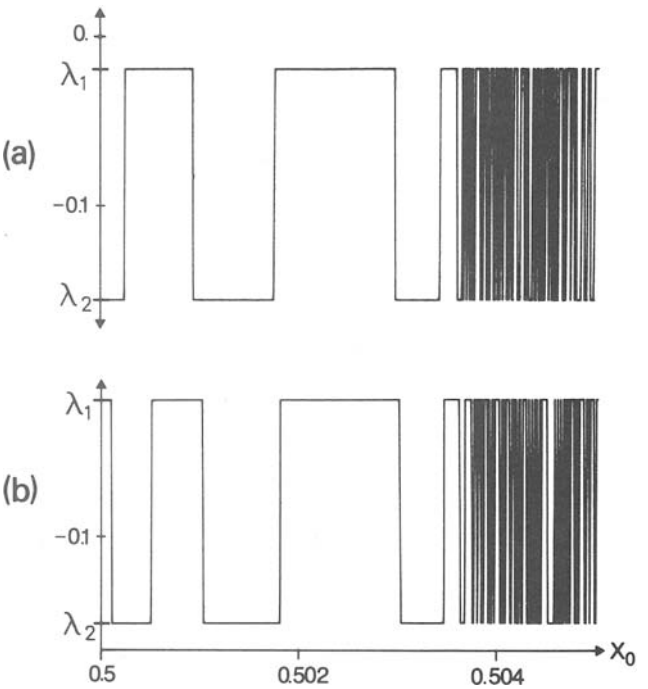

Fig.9: Same as Fig.7b, but for (a) A=3.598805; (b) A=3.598810

Noise-induced order

The phenomenon of noise-induced order is illustrated in Fig.14. Figs.14a and 14b are enlarged portions of the upper right of Figs.1a and 1b respectively. The only difference in the conditions of Figs.14a and 14b is that $p_{A|B} = 1$ (i.e. $\{r_n\} = \{BABA...\}$) in Fig.14a, and $p_{A|B} = 0.99$ in Fig.14b. In the latter case the sequence changes randomly from ABABAB... to BABABA... (repetition of B) and vice versa (repetition of A) every hundred iterations on average.

In the vicinity of the marked black cross on Fig.14b the system is ordered ($\lambda < 0$), while it is chaotic ($\lambda > 0$) in the corresponding region on Fig.14a. Thus, one may speak of "noise-induced order." At each point (i.e. A,B-pair) on Fig.14b, $N = 2 \times 10^4$ iterations were performed. A larger number of iterations would have taken a prohibitively long computing time for the whole picture. However, the effect of larger N on small subsets of Fig.14b was tested; the result was that the picture remained as shown here, except that the transition from noise-induced order to chaos became more clear cut (less fuzzy) on the A-B-plane when using more iterations.

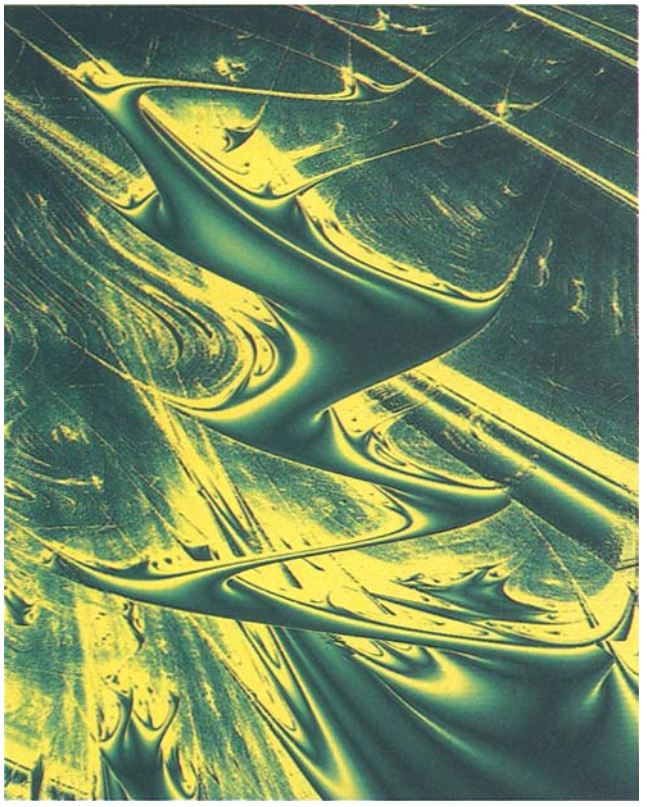

Fig.10: λ from Eq. (4). $\{r_n\} = \{BAB^2A^2B^3A^3B^2A^2BA\ BAB^2A^2B^3A^3B^2A^2BA...\}$ $x_0 = 0.8315$. Abscissa, B; ordinate, A. Ranges: $3.79302 \leqslant A \leqslant 3.93845$, $1.569 \leqslant B \leqslant 1.6017$. The color changes from dark green to yellow as λ increases from $-\infty$ to zero, and from yellow to dark green as λ increases from zero to its maximum value.

Noise-induced order, as determined here, is explained as follows. In the region around the marked cross in Fig.14b, chaos ($\lambda > 0$) coexists with order ($\lambda < 0$) in the deterministic case $p_{A|B} = 1$ (Figs.1a and 14a). The introduction of randomness allows switching from one coexisting attractor to the other, so that some sort of "average" results between the λ for order (called here λ^-) and the λ for chaos (called here λ^+). If this "average" is lower than zero, one gets noise-induced order. Fig.15 shows λ^+, λ^- and the Lyapunov exponent for $p_{A|B} = 0.99$ (called here λ_p) for fixed $A = 3.59$ and varying B. $N = 2 \times 10^5$ iterations were performed for each point on the curves. At the left part of Fig.15 only one (chaotic) attractor is obtained. In the rest of the figure, one sees that λ_p is a "rough average" of λ^+ and λ^-. Note that λ_p is larger than the arithmetic average $(\lambda^+ + \lambda^-)/2$. To explain this, we can look at Fig.16, which shows the histogram for the chaotic attractor, consisting of two regions C_L and C_R, as well as the two points of the coexisting periodic attractor. These points are indicated by two dashed vertical lines P_L and P_R. The left region C_L is reached after $r_n = B$, while the right region C_R is reached after $r_n = A$. On the other hand, the left point P_L is reached after $r_n = A$, while the right point P_R is reached after $r_n = B$. At the bottom of Fig.16, the basins of attraction for chaos (black bars) and periodicity (gaps between bars) are shown. The upper and lower bars and gaps correspond to $\{r_n\} = \{ABAB...\}$, $\{BABA...\}$. Suppose now that randomness causes a repetition of B, e.g. $\{r_n\} = \{BABAB\ BABABA...\}$. If the system is in the periodic attractor, then the point P_R is reached after BABAB. This point lies within the basin for chaos, so that the system becomes chaotic. However, if the system is chaotic, then the region C_L is reached after BABAB. This region lies only partially in the basin of attraction of periodicity, so that there is a chance that the system will

Fig.11: λ from Eq. (4). $\{r_n\} = \{B^7A^2B^9(BA)^9A^7B^2A^7\ B^7A^2B^9(BA)^9A^7B^2A^7...\}$. $x_0 = 0.8315$. Abscissa, B; ordinate, A. Ranges: $3.769 \leqslant A \leqslant 3.8175$, $1.155 \leqslant B \leqslant 1.197$. The color changes from brown to yellow as λ increases from $-\infty$ to zero, and from yellow to brown as λ increases from zero to its maximum value.

remain chaotic. The reasoning is analogous if randomness causes a repetition of A. Thus, the resulting λ_p will be larger than $(\lambda^+ + \lambda^-)/2$.

Results for Modulated Maps with a Discontinuous Maximum

This investigation is constrained to the deformations caused to the period-3 window on the A-B-plane (shown in Figs.2 to 4 for the continuous map) for different discontinuities at the maximum of the map. The iterations were performed with Eqs. (5).

The effect of $\alpha = 0.907$ is shown in Fig.17 for $\{r_n\} = \{\text{BABA...}\}$ (sequence of Fig.2), in Fig.18 for $\{r_n\} = \{\text{BBABA BBABA...}\}$ (sequence of Fig.3) and in Fig.19 for $\{r_n\} = \{\text{BBABABA BBABABA...}\}$ (sequence of Fig.4). Fig.20 displays an enlarged detail of Fig.19 (with coordinates rotated counter-clockwise by 90°, in order to take better advantage of the graphics monitor aspect ratio). Fig.21 shows an enlarged detail of Fig.20.

The consequences of a small change of $\alpha(\alpha = 0.908$, as compared to $\alpha = 0.907$ in the last paragraph) are shown in Fig.22a for $\{r_n\} = \{\text{BABA...}\}$ (sequence of Fig.17) and in Fig.22b for $\{r_n\} = \{\text{BBABA BBABA...}\}$ (sequence of Fig.18). For a better visualization of the symmetry or asymmetry with respect to the diagonal

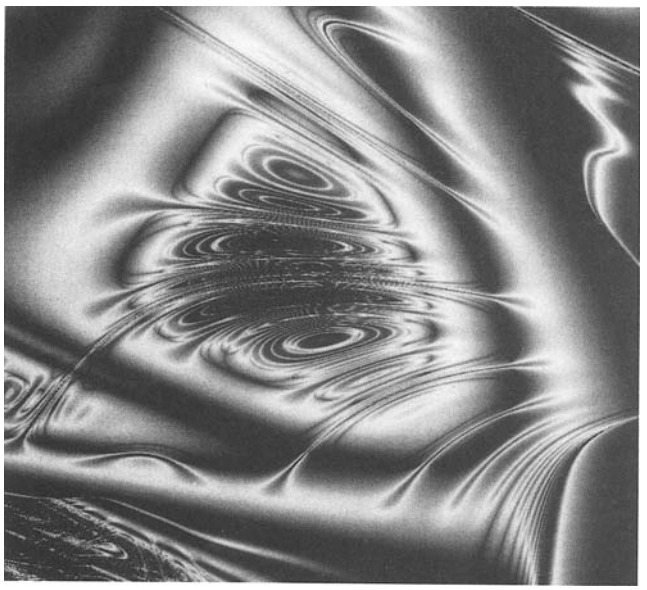

Fig.12: λ for the same equation and sequence as Fig.11, but smaller portion of the plane and x_0=0.5. Ranges: 3.7945⩽A⩽3.7989, 1.1593⩽B⩽1.16062.

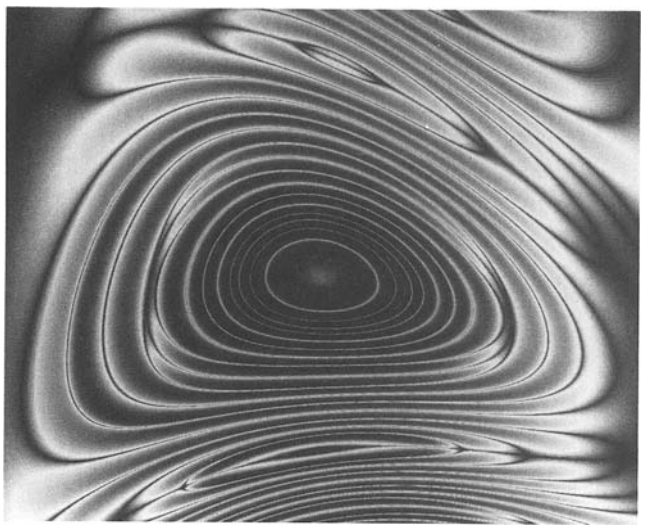

Fig.13: Enlarged portion of Fig.12. Ranges: 3.79677⩽A⩽3.79709, 1.15964⩽B⩽1.16014.

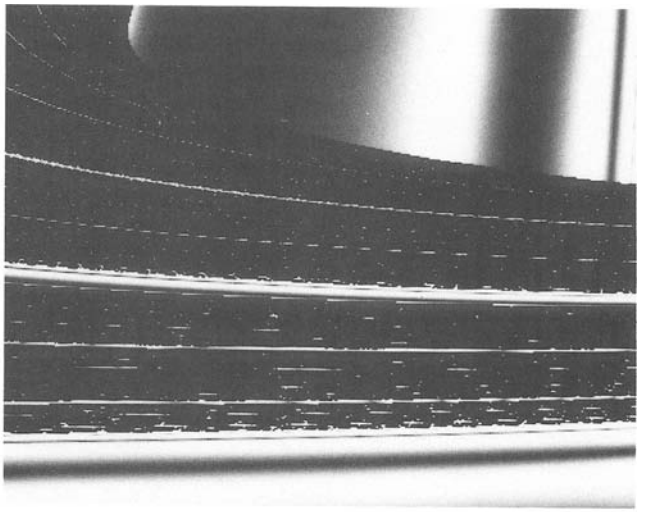

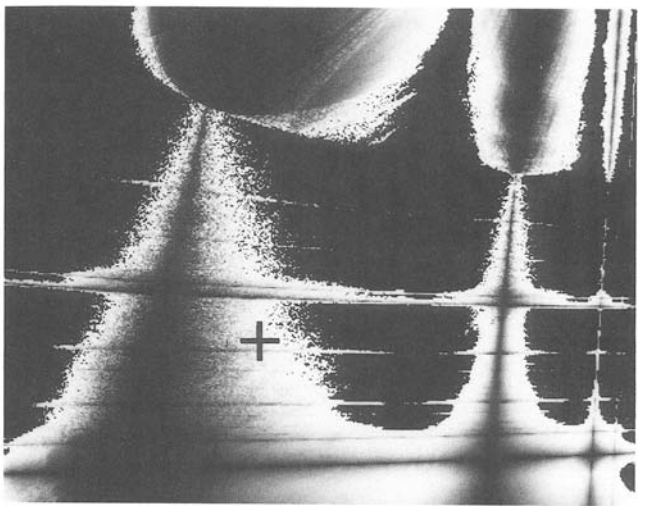

Fig.14: (a) (upper) Enlarged portion of Fig.1a; (b) (lower) Enlarged portion of Fig.1b. Ranges for (a) and (b): 3.52⩽A⩽3.78, 3.24⩽B⩽3.6.

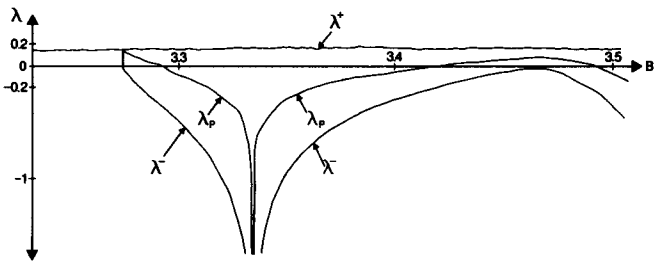

Fig.15: λ from Eq. (4) for two coexisting attractors setting $p_{A|B} = 1$ (chaotic: λ^+, periodic: λ^-) and setting $p_{A|B} = 0.99$ (λ_p). A=3.59. $p_A = p_B = 0.5$.

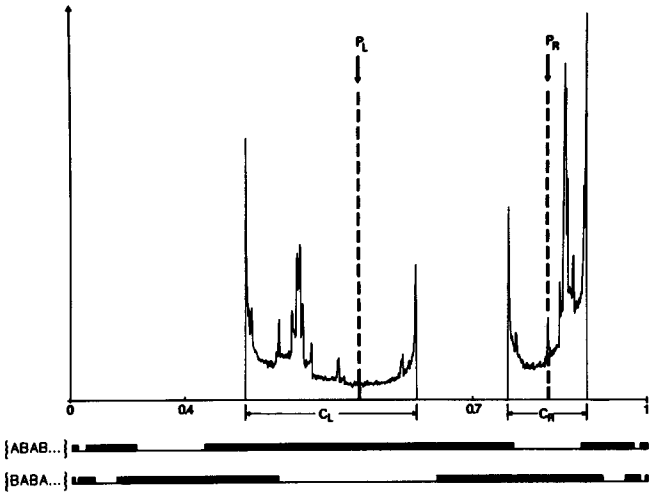

Fig.16: Histogram of a chaotic attractor (region C_L: after B; region C_R: after A) coexisting with a periodic attractor (broken lines; P_L; after A; P_R: after B). Dark bars (resp. gaps) at the bottom: basins of the chaotic (resp. periodic) attractor. A=3.59, B=3.33. $p_A = p_B = 0.5$; $p_{A|B} = 1$.

A = B, the coordinates in Fig.22 were rotated counterclockwise by 45°. Thus, the main diagonal of the A-B-plane is given by a vertical line passing through the picture center. Clearly, Fig.22a is symmetric with respect to this line, while Fig.22b is not.

A special feature of Figs.17 and 22a is the appearance of thin periodic regions (and superstable curves) for A or B approximately constant. In these regions (and curves) the dynamic properties of the system are nearly independent of B (resp. A). One example is given by the two almost straight thin bars crossing each other at the center of the lower part of Fig.22a and passing through the upper parts of the right and left picture edges. In Fig.17 (for which, in contrast to Fig.22a, the axes were not rotated) the left and lower edges (A- and B-axes) were chosen along the edges of these thin periodic regions. Figs.23 and 24 show results of calculations differing from those given in Fig.22 by the choice of α and x_0. For Fig.23, α was chosen the closest to 1 in this work. In fact, α differs in this example only by 0.65% from the value 1, which corresponds

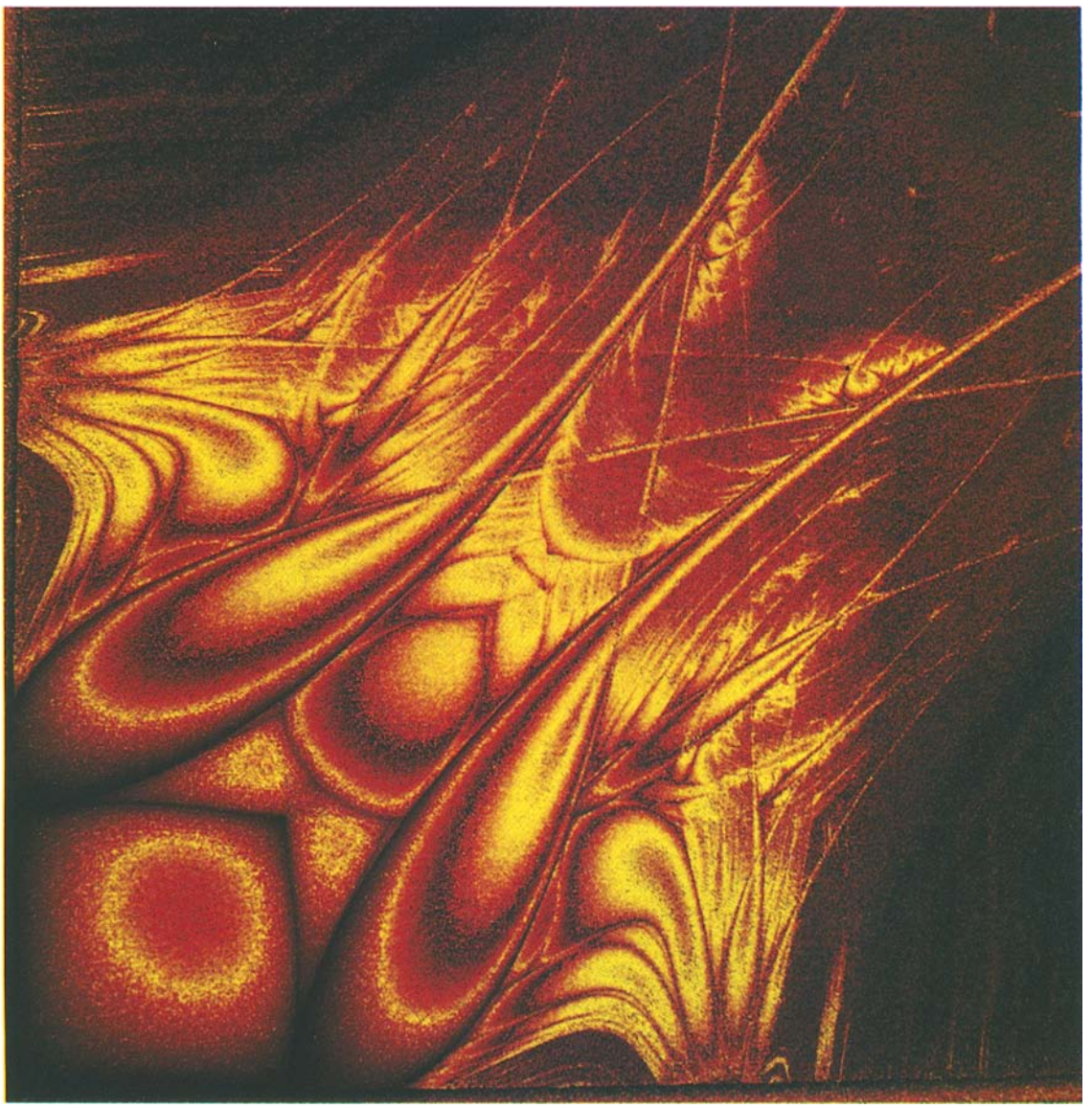

**Fig.17: λ from the discontinuous Eqs. (5). $\{r_n\} = \{BABA...\}$. $\alpha = 0.907$, $x_0 = 0.499$.
Abscissa, B; ordinate, A. Ranges: $3.8109 \leqslant A,B \leqslant 3.8207$. Different shadings of red, black and yellow alternate on increasing λ.**

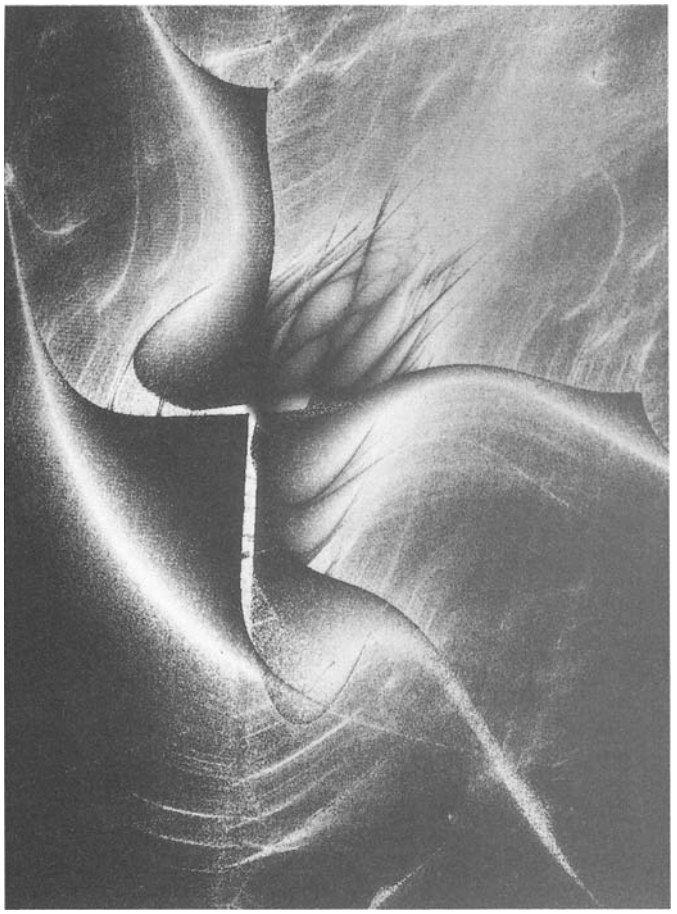

Fig.18: λ from the discontinuous Eqs. (5). $\{r_n\}=\{$BBABA BBABA...$\}$. $\alpha=0.907$, $x_0=0.499$. Abscissa, B; ordinate, A. Ranges: $3.795 \leqslant A \leqslant 3.824$, $3.80287 \leqslant B \leqslant 3.82417$.

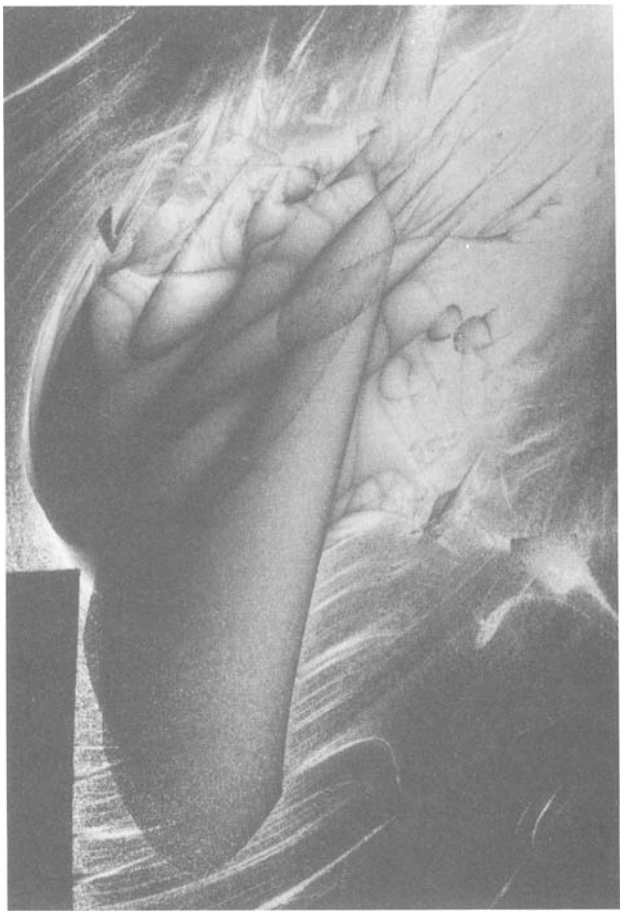

Fig.19: λ from the discontinuous Eqs. (5). $\{r_n\}=\{$BBABABA BBABABA...$\}$ $\alpha=0.907$, $x_0=0.499$. Abscissa, B; ordinate, A. Ranges: $3.80576 \leqslant A \leqslant 3.81885$, $3.8096 \leqslant B \leqslant 3.81852$.

Fig.20: Enlarged and rotated portion of Fig.19. Abscissa, A; ordinate, B. Ranges: $3.8175 \geqslant A \geqslant 3.8097$ (decreasing), $3.8138 \leqslant B \leqslant 3.8181$.

Fig.21: Enlarged portion of Fig.20. Abscissa, A; ordinate, B. Ranges: $3.81554 \geqslant A \geqslant 3.8121$ (decreasing), $3.81442 \leqslant B \leqslant 3.8177$.

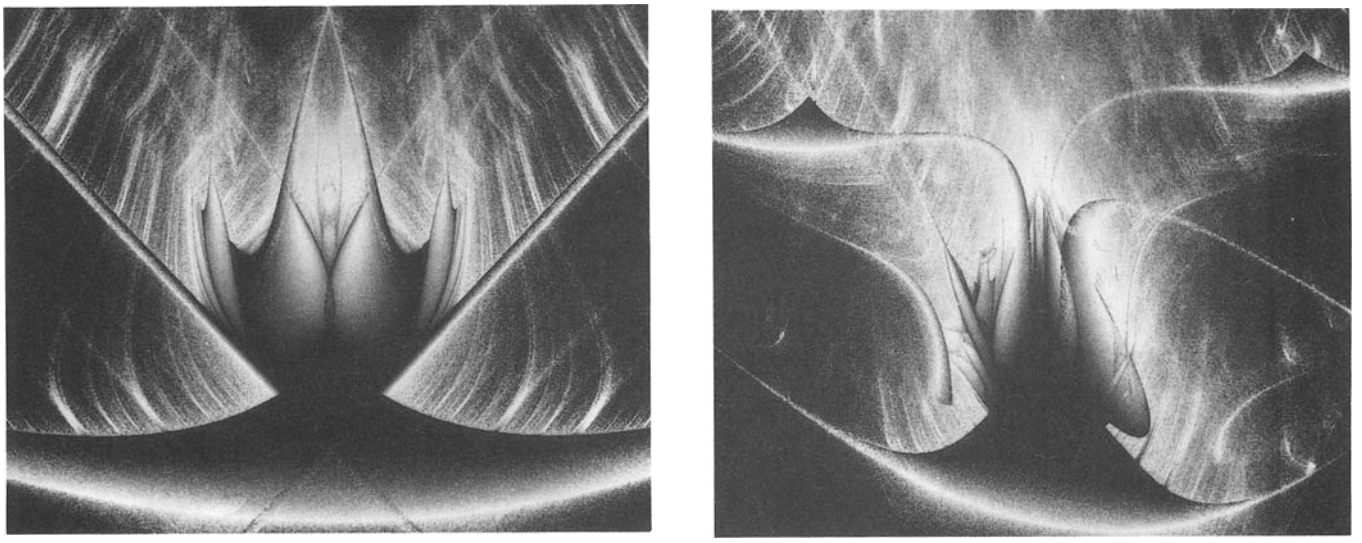

Fig.22: λ from the discontinuous Eqs. (5). $\alpha = 0.908$, $x_0 = 0.499$. Rotated coordinates. (B,A) at corners: upper left (3.8115, 3.828); upper right (3.828, 3.8115); lower right (3.8148, 3.7980). (a) (left) $\{r_n\} = \{\text{BABA...}\}$; (b) (right) $\{r_n\} = \{\text{BBABA BBABA...}\}$.

to continuity. In spite of this small discontinuity, the difference to the period-3 window obtained for the continuous case (Fig.2) is dramatic.

One can deduce that a small discontinuity at the maximum of a recurrence map, which may well appear in physical systems, considerably alters the λ(A,B)-diagrams. This is due to the breakdown of the Feigenbaum scenario, which requires a continuous maximum. Much has to be done yet to understand these diagrams. In contrast to the continuous case, the asymmetry with respect to the diagonal A = B is lost when a discontinuity is introduced for the sequence: $\{r_n\} = \{BABABA...\}$ (e.g. compare Fig.2 with Figs.17, 22a, 23 and 24). Also, self-similarity on the A-B-plane tends to disappear in the discontinuous case.

Conclusions

The graphical technique presented here allows the straightforward identification of important dynamic features: coexistence of attractors, superstable curves, noise-induced order and highly interleaved basins of attraction in phase space, as well as highly interleaved regions of different dynamic behavior in parameter space.

Highly interleaved basins of attraction have also been found in a model of glycolysis (enzymatic breakdown of sugar) based on experimental kinetic data. It was shown in that case that high interleaving of basins can lead to extreme amplification of externally applied noise[16], and that a slight periodic modulation of a control parameter can induce highly dimensional chaos[17, 18]. The simplicity of the maps in the present work allows us to understand and compute this type of phenomena in a much easier way than one would with the complicated glycolytic differential equations.

The present work illustrates five phenomena in which small deviations may have very different outcomes: (1) the sensitive dependence on initial conditions (Lyapunov

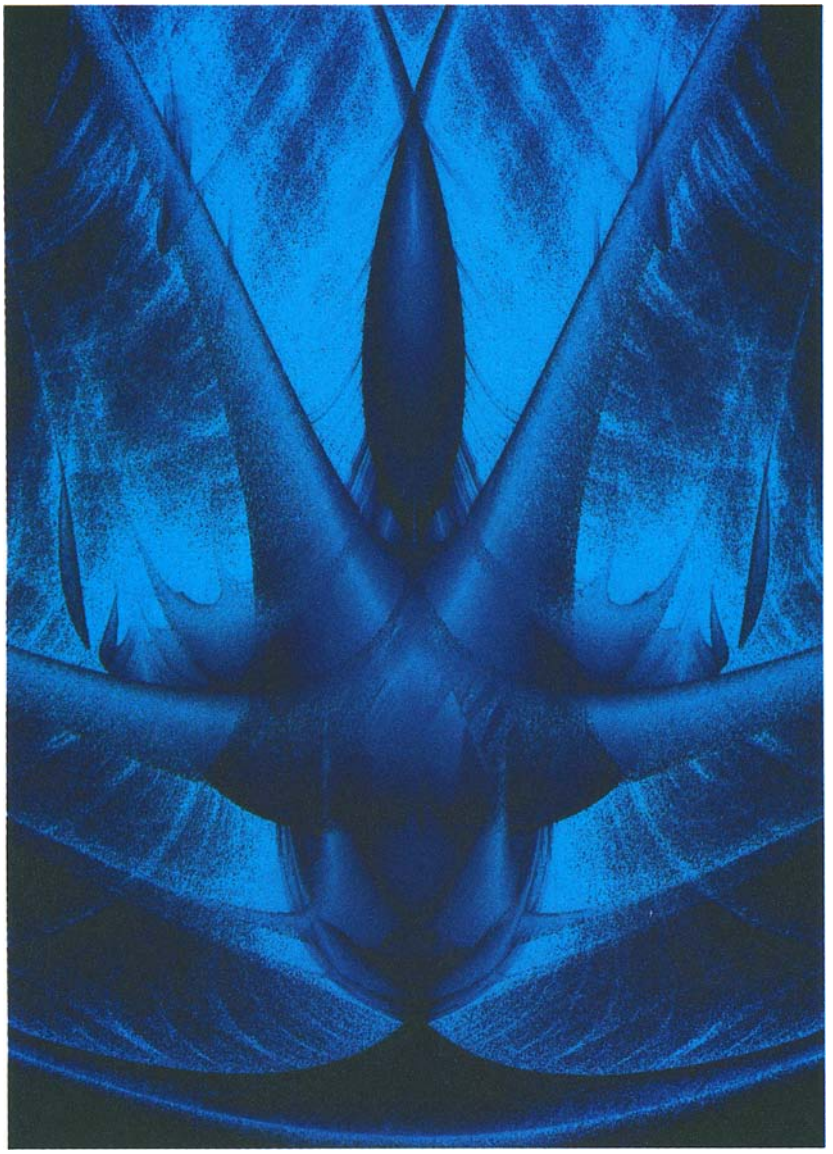

Fig.23: As Fig.22a, but $\alpha = 0.9935$, $x_0 = 0.7$. (B,A) at corners: upper left (3.8479, 3.8714); upper right (3.8714, 3.8479); lower right (3.8396, 3.8136). Dark and light shadings of blue alternate on increasing λ.

Fig.24: As Fig.22a, but $\alpha=0.8616$, $x_0=0.499$. (B,A) at corners: upper left (3.8125, 3.8276); upper right (3.8276, 3.8125); lower right (3.8053, 3.7902).

exponent $\lambda > 0$), which defines chaos in general ("butterfly effect"); (2) the sensitive dependence on initial conditions for the case of coexisting periodic attractors with highly interleaved basins in phase space (see Fig.8); (3) the sensitive dependence on control parameters which displace these highly interleaved basins in phase space (see Fig.9); (4) the sensitive dependence on control parameters for highly interleaved regions of order and chaos in parameter space (see Figs.10, 11, 24 and especially Figs.12 and 13); (5) the sensitive dependence on a discontinuity of the return map (see Figs.17–24).

Acknowledgements: I thank the Stiftung Volkswagenwerk for financial support. Also, I thank Manfred Krafczyk for enthusiastic computational assistance, Jörg Schütze for helping to find some interesting r_n-sequences at home on his personal computer, and Gesine Schulte for friendly and efficient photographic work. ■

References

1. R. M. May, Nature **261**, 459 (1976).

2. P. Collet and J. P. Eckmann, Iterated Maps on the Interval as Dynamical Systems, Progress in Physics Vol. I (Birkhäuser, Boston, 1980).

3. N. Metropolis, M. L. Stein and P. R. Stein, *J. Combinatorial Theory A*, **15**, 25 (1973).

4. S. J. Chang, M. Wortis and J. A. Wright, *Phys. Rev. A*, **24**, 2669 (1981).

5. M. Markus and B. Hess, *Comput. and Graphics*, **13**, 553 (1989).

6. J. Rössler, M. Kiwi, B. Hess and M. Markus, *Phys. Rev. A*, **39**, 5954 (1989).

7. J. Rössler, M. Kiwi and M. Markus, in: *From Chemical to Biological Organization*, edited by M. Markus, S. C. Müller and G. Nicolis (Springer-Verlag, Heidelberg, 1988), pp. 319–330.

8. M. Markus, B. Hess, J. Rössler and M. Kiwi, in: *Chaos in Biological Systems*, edited by H. Degn, A. V. Holden and L. F. Olsen (Plenum, New York, 1987), pp. 267–277.

9. M. C. de Sousa Vieira, E. Lazo and C. Tsallis, *Phys. Rev. A*, **35**, 945 (1987).

10. M. C. de Sousa Vieira and C. Tsallis, in: *Instabilities and Nonequilibrium Structures II*, edited by E. Tirapegui and D. Villarroel (Kluwer Acad. Publ., 1989), pp. 75–88.

11. P. Szépfalusy and T. Tél, *Physica D*, **16**, 252 (1985); Z. Kaufmann, P. Szépfalusy and T. Tél (unpublished).

12. Harwell Subroutine Library (1973). A Catalogue of Subroutines. Theoretical Physics Division, A.E.R.E., Harwell, England.

13. L. Glass and R. Pérez, *Phys. Rev. Lett.*, **48**, 1772 (1982).

14. J. Bélair and L. Glass, *Phys. Lett. A*, **96**, 113 (1983).

15. J. Bélair and L. Glass, *Physica* **16D**, 143 (1985).

16. B. Hess and M. Markus, Ber. Bunsenges. *Phys. Chem.*, **89**, 642 (1985).

17. B. Hess and M. Markus, in: *Temporal Order*, edited by L. Rensing and N.I. Jaeger (Springer-Verlag, Heidelberg, 1985), pp. 179–190.

18. M. Markus and B. Hess, *Arch. Biol. Med. Exp.*, **18**, 261 (1985).